DUJASE Vol. 5(1 & 2) 9-12, 2020 (January & July)

Performance Study of an Interdigitated Back Contact Si Solar Cell using TCAD

Koushik Kumar, Ron Saha and Mainul Hossain*

Department of Electrical and Electronic Engineering, University of Dhaka, Dhaka-1000, Bangladesh

**E-mail: mainul.eee@du.ac.bd*

Received on 07 May 2020, Accepted for publication on 10 September 2020

ABSTRACT

In this study, a functional interdigitated back contact heterojunction silicon solar cell (IBC-SHJ) was designed and its electrical characteristics were analyzed using technology computer aided (TCAD) device simulation tool. Having rear contacts exposes the entire front surface of an IBC-SHJ solar cell to the solar spectrum, thereby, enabling it to attain higher efficiency compared to traditional solar cells with front contacts. Performance of the IBC-SHJ cell was rigorously studied with respect to the thickness and material of the antireflective coating (ARC) as well changing doping concentration of amorphous silicon (a-Si) layer. The efficiency (η) of the proposed design is extracted from the characteristic I-V curves under various conditions. Optimizing the design parameters, a maximum efficiency of ~25% was achieved for 200nm thick Si_3N_4 ARC and with a doping concentration of $10^{20}cm^{-3}$ in the a-Si layer. The results obtained from this simulation study were found to be consistent with experimental data available in the literature.

Keywords: IBC solar cell, TCAD, modeling.

1. Introduction

An interdigitated back contact hetero-junction silicon solar cell (IBC-SHJ) combines back contact architecture with simple hetero-junction solar cell design [1 - 2]. Compared to conventional solar cells, all metal contacts in an IBC solar cell are placed on the rear surface. Consequently, the whole front surface is exposed to illumination, eliminating absorption and reflection losses from the contacts and, thereby, generating higher short-circuit current (J_{sc}). Moreover, as the contacts are in the rear surface, various texturing and light trapping structures can be introduced in the front surface to ensure more electron-hole pair generation [3].

The basic design and cross-section of a conventional IBC-SHJ solar cell is shown in Fig. 1. The heterojunction structure enables the cell to absorb energies from a wider range of the solar spectrum. Since the IBC structure has heavily doped junctions, high-intensity saturation effects will be minimum until open-circuit voltage (V_{oc}) becomes comparable to the band gap potential. The front surface of the cell is of n-type crystalline silicon (c-Si) and the rear side consists of heavily doped alternating, p+ and n+ regions. Metal contacts, made of aluminum, are placed directly below the amorphous silicon(a-Si) region. Electron-hole pairs are generated in the c-Si when the front surface is illuminated. Some of these electron hole pairs recombine and some contribute to current based on diffusion length and drift properties. In a n and n+ junction, the lightly doped n region works serves as hole and electron abundant regions, respectively. So, the holes move to n+ region due to the electric field and get collected on cathode. Similarly, in p+ and n+ region, due to the electric field, electrons drift to p+ and get collected in cathode and contribute to the photocurrent. The conventional fabrication process of the IBC cell includes the local diffusion of boron (B) at the back surface followed by a local diffusion of phosphorous, resulting in an alternating layer of p and n junctions. The key to increasing the efficiency is to ensure that a high number of electrons and holes are collected in their respective contacts. To do so, the bulk minority carrier lifetime, or diffusion length must be significantly large. To provide the lowest surface recombination, optimizing of a buffer layer for surface passivation is required. Also, the structure of the rear side (pitch, p-type emitter, n-type Back surface field (BSF) and gap width) should be optimized so that the series resistance can be minimum.

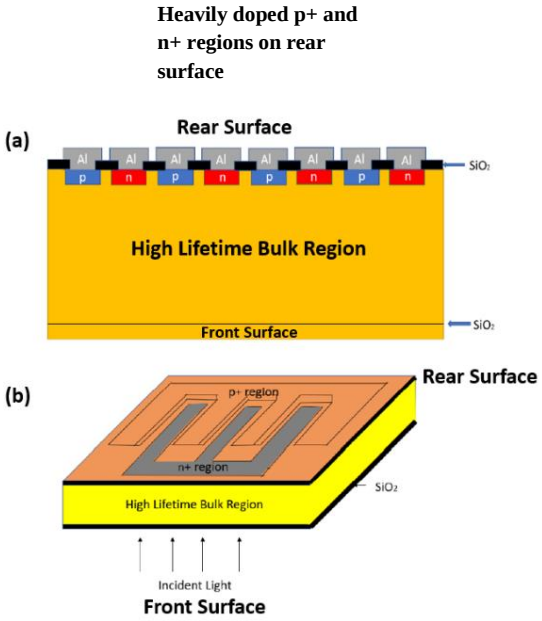

Fig. 1: (a) Basic design of IBC-SHJ solar cell (b) Cross-Section

2. Related Work

IBC solar cells have gained a lot of interest in recent times owing to their high-power conversion efficiencies (PCE). Yoshikawa *et al.* also achieved PCE over 26%, using high-quality thin-film HJ (hetero-junction) passivation techniques and electrodes with low contact resistance. A loss analysis

was done which points to a path where conversion efficiency of 29% can be achieved [4]. Tasmiat *et al.* described efficient techniques to increase minority carrier lifetime from 460μs to 1.8ms during the fabrication of IBC solar cells [5]. Lately, TCAD simulations have shown that IBC solar cells with

MgF_2 anti-reflection coatings (ARCs) can achieve a record PCE of 26.6% [6]. Despite many studies to boost IBC solar cell performance, little effort has been made to understand how ARC materials influence device behavior in IBC solar cells.

In this study, cell using technology computer aided (TCAD) device simulation tool to study the influence of ARC material and thickness on IBC solar cell performance were tested/ studied. Moreover, I-V characteristics using different concentrations of dopants in the a-Si layer is also studied.

3. Simulation Model

Silvaco ATLAS simulator solves three basic equations of semiconductor which are: Poisson's equation, Carrier Continuity Equations, Fermi-Dirac, and Boltzmann Statistics. These equations are also used in modeling the cell performance in simulation [2]. The relation between the electrostatic potential (ψ) and the space charge density (ρ) is given by Poisson's Equation, as follows:

$$div(\varepsilon \nabla \psi) = -\rho \quad (1)$$

Here, ε = permittivity of the medium. All the mobile and fixed charges, including free carriers (e^- and h^+) and ionized impurities, are represented by the local space charge density. The career continuity equations are given as:

$$\frac{\delta n}{\delta t} = \frac{1}{q} div \boldsymbol{J_n} + G_n - R_n \quad (2)$$

$$\frac{\delta p}{\delta t} = \frac{1}{q} div \boldsymbol{J_p} + G_p - R_p \quad (3)$$

where the electron and hole concentrations are given by n and p, respectively. Current density (J), generation rate (G) and recombination rate (R) and electron charge (q) are represented by their usual symbols. The standard drift-diffusion model gives the value of electron and hole current densities:

$$\boldsymbol{J_n} = q\mu_n nE + qD_n \nabla n(x) \quad (4)$$

$$\boldsymbol{J_p} = q\mu_p pE - qD_p \nabla p(x) \quad (5)$$

where μ_n= electron mobility μ_p= hole mobility, E = electric field, D_p= diffusion coefficient for holes and D_n = diffusion coefficient for electrons. Different electron hole pair recombination models are used while simulating this IBC solar cell structure. These models are Shockley-Read-Hall recombination model (RSRH), Klaassen mobility model and Auger recombination model. The equations [5-8] for these models are given below respectively.

$$RSRH = \frac{pn - n_{ie}^2}{\tau_p[n + n_{ie}] + \tau_n[p + n_{ie}]} \quad (6)$$

$$\mu_{no}^{-1} = \mu_{nL}^{-1} + \mu_{nDAP}^{-1} \quad (7)$$

$$R_{Auger} = 2.8 \times 10^{-31}(pn^2 - n_{nie}^2) + 9.9 \times 10^{-32}(np^2 - p_{nie}^2) \quad (8)$$

For the device structure shown in Fig. 1, 2D simulations, that are consistent with practical devices, are carried out using SILVACO ATLAS device simulation tool. Fig. 2 shows the detailed simulation process flow. Table I shows the parameters used in device simulations. To generate the photocarriers in the cell, a beam statement has been used where sun power has been taken as 700W/m^2, with the sun`s rays perpendicular to the front surface.

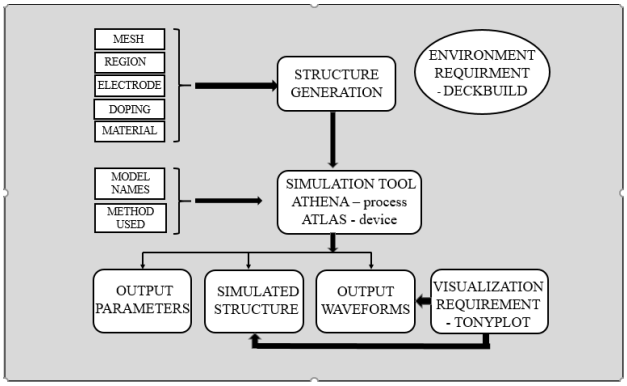

Fig. 2: Flowchart of device simulation using SILVACO TCAD

Table I: Simulation Parameters

Parameter	Value
Electron recombination lifetime	10^{-6}s
Hole recombination lifetime	10^{-6}s
c-Si, n doping at 300K	10^{17}cm^{-3}
Energy gap at 300K	1.7 eV
Electron mobility	1cm^2/Vs
Hole mobility	0.1 cm^2/Vs

Gaussian intensity distribution over the front surface has been considered. The peak intensity is 1000W/m^2 or 1 sun (standard test condition). After the coordinate of the beam statement is set 50μm, a distribution matrix covering the whole front surface is created. The software internally sets intensity values at every point.

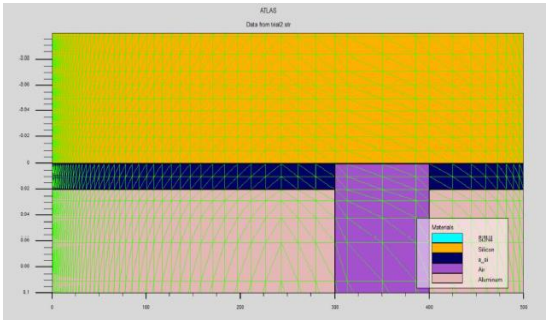

Fig. 3: Meshing in IBC-SHJ solar cell

The meshing of the structure is carefully defined. Surfaces where the dopants are added, and where detailed analysis are required, require finer mesh size. Hence, the depth of mesh is higher in the junction region and lower in the bulk semiconductor region, as shown in Fig. 3. A smaller mesh

size improves the accuracy of the simulations but increases computational time. Therefore, a tradeoff must be made between accuracy and faster turn-around. At last, a voltage sweep, with a step size of 0.05 V, is conducted at the emitter terminal that calculates the current values from V = 0 V to 0.8 V.

4. Results and Discussion

4.1. Generation Profile of the Carriers

The generation profile for the carriers, in the illuminated IBC-SHJ solar cell, was obtained using TCAD. Fig. 4 shows the schematic view of the photo generation in the IBC solar cell, showing the rate at which photo carriers are generated as the solar radiation is incident on the front surface.

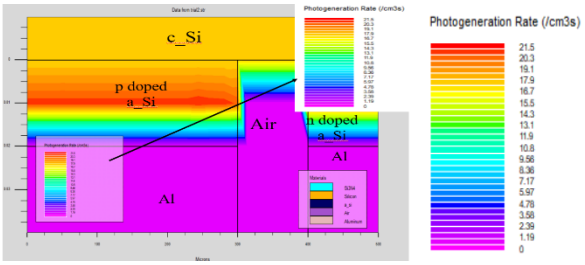

Fig. 4: Carrier Generation Profile

There are plenty of photo carriers in the bulk region and in the a-Si region. But the rate of generation has been gradually decreasing with the depth of the structure and it becomes eventually zero in the contact material along the rear side of the junction.

4.2. Variation in ARC material

The J_{sc}-V_{oc} characteristics of the IBC cell was investigated for commonly used single layer ARC materials: Si_3N_4, Al_2O_3, SiO_2 and TiO_2. The results are shown in Fig. 5 with efficiency plots in the inset.

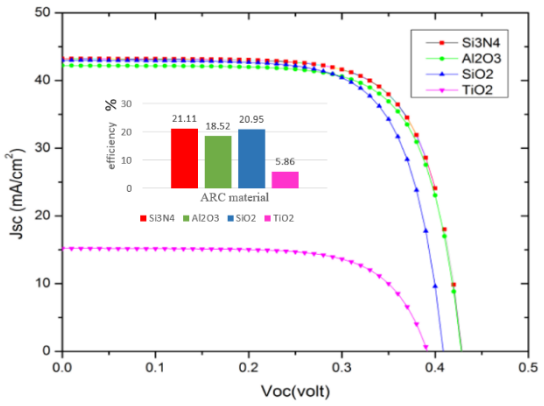

Fig. 5: J_{sc}-V_{oc} characteristics and efficiency of IBC solar cell with commonly used ARC

The thickness of each layer was taken as 200nm, which is the standard in most IBCs. The n+ and p+ doping in the a-Si layer is 10^{21} cm^{-3}. Based on the results, it is obvious that for the same thickness, Si_3N_4 provides the highest efficiency and there acts as the best ARC material. At any given wavelength, anti-reflection properties depend on specific thickness, refractive index, and transparency. Table II shows the refractive indices of the index of the materials [8].

Table II: Refractive Index of ARC

ARC Material	Refractive Index
Si_3N_4	1.9
Al_2O_3	1.652, 1.656
SiO_2	1.4, 1.5
TiO_2	2.3

As described by Hedayati *et al.* [10], if $n_s$is the refractive index of a non-absorbing surface, at any given wavelength, λ, then the refractive index of the ARC material should be

$$n_{ARC} = \sqrt{n_s . n_{env}} \tag{9}$$

to obtain zero reflection at that λ. Here, n_{env} is the refractive index of the surrounding environment. Also, for zero reflection at that λ, the corresponding thickness of the ARC material, d_{ARC}, must meet the following criterion:

$$d_{ARC} = \frac{\lambda}{4 n_{ARC}} \tag{10}$$

For instance, at a wavelength of 550nm, silicon will need a 68 nm thick ARC with a refractive index of 2.02, to minimize reflection [10]. The preferred ARC will therefore be Si_3N_4 as seen from the refractive index values in Table II.

4.2. Variation in ARC thickness

Here, we investigate how the J_{sc}-V_{oc}characteristics of the IBC change for different thickness of the $S_{i3}N_4$. The results are illustrated in Fig. 6 with the efficiency % shown in the inset:

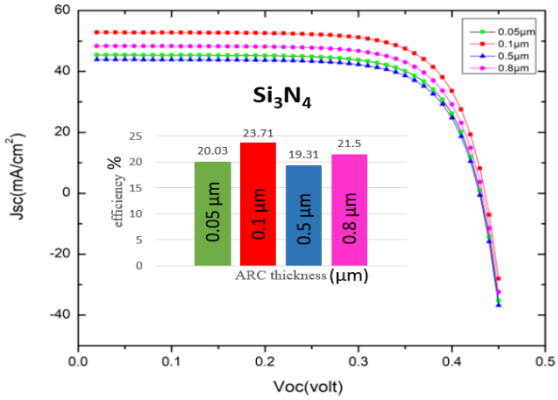

Fig. 6: J_{sc}-V_{oc} characteristics and efficiency of IBC solar cell at varying thickness of Si_3N_4 ARC coating

With the increase of ARC thickness from 0.05μm to 0.1μm the short-circuit current increased from 45.41 mA/cm^2 to52.79mA/cm^2. This is because, a thicker ARC has significantly reduced the reflection on the front surface and increased absorption on the bulk semiconductor. Highest efficiency was found for an optimum Si_3N_4 thickness of 0.1μm (100nm). If the thickness is higher or lower than 0.1μm, then the photo carriers are lost either in the ARC layeror in the bulk region.

4.3. Variation doing concentration in a-Si

We have also studied how the doping concentration in the a-Si layer changes the I-V behavior of the IBC solar cell. 200nm of Si_3N_4 is chosen as the ARC. The results are shown in Fig. 7.

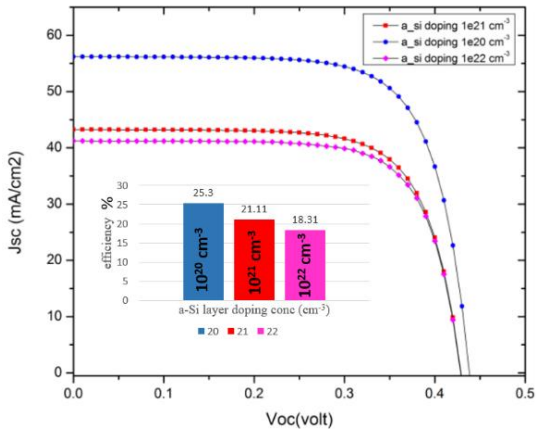

Fig. 7: I-V characteristics and efficiency of IBC solar cell at varying doping concentration in a-Si layer

As doping concentration decreases, the short-circuit current increases. This happens because of the huge difference in doping profile of the bulk c-Si and the a-Si. As the doping profile of a-Si is 1000-10,000 times higher than c-Si, the depletion region penetrates deeper into the c-Si side. As a result, electron scattering will occur in the p+ type of a-Si, reducing electron and hole mobility. Consequently, carrier recombination increases and thus current density decreases. Reducing the difference of doping profile mitigates the problem to a certain permissible value and vice versa. Maximum efficiency of 25% was achieved when the doping concentration in the a-Si layer was $10^{20}cm^{-3}$.

5. Conclusion

In this report we have successfully depicted the designed IBC-SHJ solar cell using TCAD simulation tool. The influence of several parameters, like the type and thickness of ARC material, doping concentration in the a-Si layer, on the device performance have been thoroughly studied. Optimizing these parameters an efficiency of ~25% was obtained with 200 nm thick Si_3N_4 as the ARC, with a doping concentration of $10^{20}cm^{-3}$ in the a-Si layer. The future work will focus on developing a 3D model of the IBC-SHJ solar cell and make a more comprehensive study of the parameters to further optimize the performance. Moreover, we plan to design and model IBC-SHJ solar cells with front surface texturing to achieve a boost in the efficiency.

References

1. Z. Shu, U. Das, J. Allen, R. Birkmire, and S. Hegedus, *Experimental and simulated analysis of front versus all back-contact silicon heterojunction solar cells: Effect of interface and doped a-Si:H layer defects*,Prog Photovolt Res Appl.,23, 78–93, 2015.

2. M. Belarbi, M. Beghdad, and A. Mekemeche, *Simulation and optimization of n-type interdigitated back contact silicon heterojunction (IBC-SiHJ) solar cell structure using Silvaco TCAD Atlas*,Sol. Energy, 127, 206–215, 2016.

3. D. Eisenhauer, C.T. Trinh, D. Amkreutz and C. Beckera, *Light management in crystalline silicon thin-film solar cells with imprint textured glass superstrate*, Sol. Energy Mater. Sol. Cells, 200, 109928, 2019.

4. K. Yoshikawa *et al*., *Silicon heterojunction solar cell with interdigitated back contacts for a photoconversion efficiency over 26%*, Nat. Energy, 2, 17032, 2017.

5. T. Rahman *et al*., Minimising bulk lifetime degradation during the processing of interdigitated back contact silicon solar cells,*Minimising bulk lifetime degradation during the processing of interdigitated back contact silicon solar cells*, Prog Photovolt Res Appl., 26, 38-47, 2018.

6. M. Pomaska *et al*., *Transparent silicon carbide/tunnel SiO_2passivation for c-Sisolar cell front side: Enabling J_{sc}> 42 mA/cm^{2}and iV_{oc}of742 mV*, Prog Photovolt Res Appl., 28, 321–327, 2020.

7. V. Budhraja, S. Devayajanam, and P. Basnyat, *Simulation Results: Optimization of Contact Ratio for Interdigitated Back-Contact Solar Cells*, Int. J. Photoenergy,7818914, 2017.

8. L. J. Koduvelikulathu*et al*., K. Peter, *2-D Modeling of n-Type IBC Solar Cells Using SILVACO ATLAS Simulation*, Handbook of Optoelectronic Device Modeling and Simulation, 3–4, 2011.

9. L.A. Dobrzański and M. Szindler, *Al_2O_3 antireflection coatings for silicon solar cells*, J. Achiev. Mater.Manuf. Eng., 59, 13-19, 2013.

10. M.K. Hedayati, and M. Elbahri, *Antireflective Coatings: Conventional Stacking Layers and Ultrathin Plasmonic Metasurfaces, A Mini-Review*, Materials, 9, 2016.